science.sciencemag.org/content/368/6493/874/suppl/DC1

Supplementary Materials for

Precise pitch-scaling of carbon nanotube arrays within three-dimensional DNA nanotrenches

Wei Sun*†, Jie Shen†, Zhao Zhao†, Noel Arellano, Charles Rettner, Jianshi Tang, Tianyang Cao, Zhiyu Zhou, Toan Ta, Jason K. Streit, Jeffrey A. Fagan, Thomas Schaus, Ming Zheng, Shu-Jen Han, William M. Shih, Hareem T. Maune, Peng Yin*

*Corresponding author. Email: py@hms.harvard.edu (P.Y.); sunwedaivd1@gmail.com (W.S.)
†These authors contributed equally to this work.

Published 22 May 2020, *Science* **368**, 874 (2020)
DOI: 10.1126/science.aaz7440

This PDF file includes:

Contents

S1 Materials and experimental methods

S1.1 Assembly of DNA templates

Assembly of the designed DNA templates followed a multistage isothermal reaction. In brief, 90 μL mixture of unpurified DNA bricks (IDTDNA Inc., pH 7.9, containing 300 – 600 nM of each brick, without careful adjustment of each brick stoichiometry), 5 mM Tris, 1 mM EDTA, and 40 mM $MgCl_2$ was incubated at 80°C for 15 min, 44°C for 12 h, 39°C for 72 h, and 31°C for 8 h sequentially. The as-synthesized DNA templates were used without further purification.

S1.2 Wrapping CNTs with DNA

Semiconducting CNT-enriched powder was directly purchased from NanoIntegris. The labeled purity for semiconducting CNTs was ∼95%, and the powder was used without further purification. Wrapping single-stranded DNAs onto CNT surface followed previous reports (*27, 28*).

First, strand L1 (25 μM, sequence: 5′–GATGCGAGGCTATTCTGTGTGTGTGTGTGTGTGTGTGTGTGTGTGTGTGT GTGTGTGT–3′) was mixed with CNT powder (0.1 mg) in buffer (1× TBE and 100 mM NaCl at pH 8.3). The mixture was sonicated for 1h, followed by high-speed centrifuge at 16,000 g for 30 min to remove aggregates. The supernatant solution was then purified using 100 kD Amicon filter (EMD Millipore) to get rid of excessive DNAs. Strand L2 (10 μM, sequence: 5′–AGAATAGCCTCGCATCCCACTTACCACTTA–3′) was added to the purified CNT-L1 sample and annealed from 37°C to 23°C within 2 h, followed by incubation at 23°C for 16 h. L2-wrapped CNTs were used without further purification. Notably, all the CNTs used in the manuscript exhibited irregular lengths.

We also tested using the electric arc CNTs (CNT powder, containing both metallic and semiconducting CNTs, were purchased from Carbon Solutions, Inc.). Semiconducting CNTs were purified and enriched using previously published method (*33*). The purity for the enriched semiconducting CNTs was ∼95%. The method for wrapping DNAs onto the enriched semiconducting CNTs was identical to the method above. Note, after wrapping L1, we purified the L1-wrapped CNTs by a surfactant/DNA exchange process according to the previous published method (*34*).

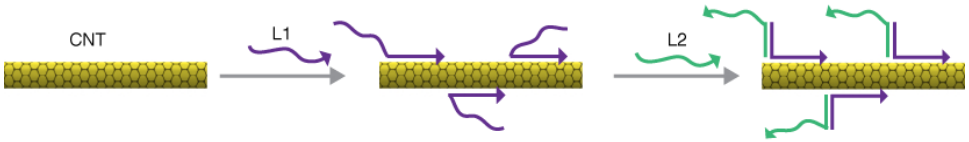

Figure S1. **Schematic for two-step DNA wrapping around CNTs.**

S1.3 Assembly of CNT arrays on DNA templates

L2-wrapped CNTs (0.4 μL) were mixed with 0.4 μL diluted DNA templates (10× dilution into 15 mM $MgCl_2$ solution) into 6 μL final solution containing 10 mM $MgCl_2$ and 400 mM NaCl (for 24-nm inter-CNT pitch sample) or 10 mM $MgCl_2$, 300 mM NaCl, and 300 mM LiCl (for 16-/12-/10-nm inter-CNT pitch sample). The reaction buffer was incubated at 33°C for 9 h, and then stored at 4°C without further purification.

S1.4 Buffer conditions

For the assembly of DNA brick crystals and DNA-wrapped CNTs, the buffer solutions were used according to previous reports (*17, 28*). For the assembly of CNTs on DNA brick crystals with 24 nm inter-CNT pitch, we used a buffer solution containing 10 mM $MgCl_2$ and 400 mM NaCl. Without NaCl, DNA-wrapped CNTs may aggregate during the incubation at 33°C. For 16-/12-/10-nm pitch DNA brick crystals, we further introduced lithium ion (300 mM) into the buffer to lower the electrostatic repulsions between the negatively charged DNA helices and CNTs.

S1.5 Transmission electron microscopy (TEM)

0.6 μL as-prepared (without purification) DNA templates solution or CNT-decorated DNA templates solution was diluted into 5 μL water and adsorbed onto glow discharged carbon-coated TEM grids for 4 min. Then the remaining solution was wiped away, followed by negative staining using 6 μL 2 % aqueous uranyl formate solution (7 sec) and a quick water rinsing. Imaging was performed using an JEOL 1200 operated at 80 kV.

S1.6 Atomic force microscopy (AFM)

7 μL as-prepared DNA templates solution or CNT-decorated DNA templates solution was deposited onto a 1-cm^2 sized silicon chip followed by stepwise rinsing in 50%, 95%, and 99.5% ethanol. The sample was imaged on a Multimode SPM (Vecco) *via* tapping mode.

S1.7 DNA removal and FET construction

The following five-step fabrication process is used to remove surface DNA, clean the substrate, and construct the electrodes onto CNTs: (1) a low resolution (>912 magnification) SEM imaging (LEO 1550) at 10 keV to identify the suitable areas for device fabrication; (2) fabricating fine alignment markers with e-beam lithography around the selected CNT arrays; (3) thermal annealing of the Si substrate at 550°C under Argon to clean the substrate and to reduce the DNA thickness; (4) using AFM (peak force mode) for precise registration of the assembled CNTs with respect to the fiducial markers; and (5) two-step e-beam lithography for fabricating the contact electrodes onto the assembled CNT arrays and electrical pads. Notably, after step 3, the surface roughness of the substrate is reduced from 1 nm before cleaning to 0.3 nm after cleaning. And the thickness of the DNA residues is reduced to less than 1 nm.

Fine alignment markers and thermal annealing:

A 200-nm thick PMMA layer is spun onto the Si wafer and the fine alignment marker pattern is written using Leica ebeam VB6 HR tool (a current of 0.5 nA at a dose of 1800 μC/cm^2). The alignment marker pattern is developed in a 1:3 mixture of MIBK and IPA. A 10-nm thick titanium film is deposited using thermal evaporation in a homebuilt evaporator. Liftoff is performed at room temperature in acetone without sonication followed by an IPA rinse and the sample is dried with Nitrogen. Finally, thermal annealing is performed using rapid thermal annealing (AccuThermo) tool with 20 psi Argon at 1 slm/min flow rate under 550°C for 30 minutes. Notably, writing the markers before or after DNA deposition does not significantly affect the effectiveness of DNA removal.

Two-step e-beam lithography for electrical contacts onto CNTs:

A 200-nm thick PMMA is spun onto the Si wafer and the fine electrical contact pattern is written using Leica ebeam VB6 HR tool (a current of 0.5 nA at a dose of 1800 μC/cm^2). The contact pattern is developed in a 1:3 mixture of MIBK and IPA, and then dried with compressed Nitrogen. To remove any residual DNA prior to metal deposition, sample is dipped in DNA Exitus Plus (AppliChem) solution for 15 sec followed by a DI water rinse and a quick dip (2 sec) in HCl followed by DI water rinse, then dried with Nitrogen. A stacking metal film of 1-nm thick titanium, 20-nm thick palladium, and 10-nm thick gold is deposited using thermal evaporation on a homebuilt evaporator. Liftoff is performed at room temperature in acetone without sonication, followed by an IPA rinse, and the sample is dried with Nitrogen.

For large electrical contact pads connecting to the fine electrical contacts, a 450-nm thick PMMA is spun onto the sample. Proximity corrected contact pad pattern is exposed using Leica ebeam VB6 HR tool with a current of 5 nA and dose depending on the area within the pattern. The contact pads pattern are developed in a 1:3 mixture of MIBK and IPA, then dried with compressed Nitrogen. A stacking metal film of 5-nm thick titanium and 50-nm thick gold is deposited using thermal evaporation on a homebuilt evaporator. Liftoff is performed at room temperature in acetone without sonication, followed by an IPA rinse, and the sample is dried with Nitrogen.

Electrical measurements on CNT FETs:

The electrical measurements on the constructed CNT FETs are performed at room temperature in a vacuum probe station connected to an Agilent B1500A Semiconductor Device Analyzer.

S2 Extended technical details of CNT-alignment quality

S2.1 Extended technical details for CNT assembly yield analysis

Assembly yield was estimated using TEM images. Assembly yield was defined as the total inner nanotrenches occupied by the correctly formed parallel CNT arrays over the total numbers of inner DNA nanotrenches. Two peripheral DNA nanotrenches on the boundaries were excluded considering the incomplete crystal formation on the growing edges. CNTs on 10 randomly selected DNA brick crystals were counted.

In the TEM images, the following occupation status for DNA nanotrenches were observed: (1) DNA trench contains one CNT, aligned along the longitudinal axis of the nanotrench, (2) DNA trench contains multiple CNTs, aligned along the longitudinal axis of the nanotrench, and CNTs are in the end-to-end conformation, (3) empty DNA trench. In our calculation, both (1) and (2) were considered as the trenches correctly occupied by the aligned CNTs.

$$\text{Assembly Yield} = \frac{\text{Number}_{\text{Trenches with aligned CNTs}}}{\text{Number}_{\text{Total inner trenches}}}$$

Notably, because we haven't observed the crossing or the bundling of CNTs within the DNA trenches, the assembly yield does not include these typical misalignment defects. Hence, the definition of assembly yield does not over-estimate the yield for forming the uniform parallel CNT arrays.

S2.2 Extended technical details for CNT orientation analysis

CNT orientation was estimated using TEM images. The angular deviation of CNTs was defined as the difference between the longitudinal axis of CNT and the longitudinal axis of DNA nanotrenches. CNTs on 10 randomly selected DNA brick crystals were analyzed.

S2.3 Extended technical details for the variation of inter-CNT pitch

The range of inter-CNT pitch variation was defined as the difference between the maximum and minimum pitch values of adjacent CNTs. And the percent relative range of the inter-CNT pitch, defined as the range of inter-CNT pitch divided by the average value of inter-CNT pitch. The inter-CNT pitch was measured on TEM images. And CNTs on 10 randomly selected DNA brick crystals were measured. For every two neighboring CNTs, we measured three different positions along the longitudinal axis of CNT.

S3 Design and characterization of DNA brick crystal templates

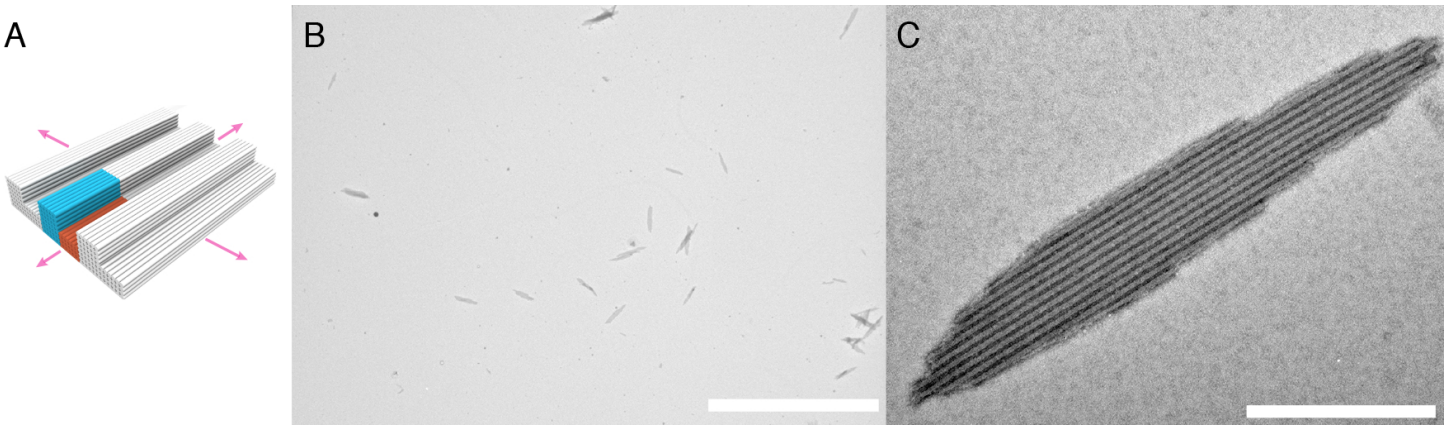

Figure S2. **Design (A), zoomed-out (B), and zoomed-in (C) TEM images of the DNA brick crystal with 25.3-nm trench periodicity along x direction**. Feature-repeating unit of the designed crystal is denoted using colored bundles. Pink arrows in A represent the growth directions of the crystal template. DNA brick crystals are diluted 500 folds prior to imaging. The scale bar in B is 10 μm. The scale bar in C is 500 nm.

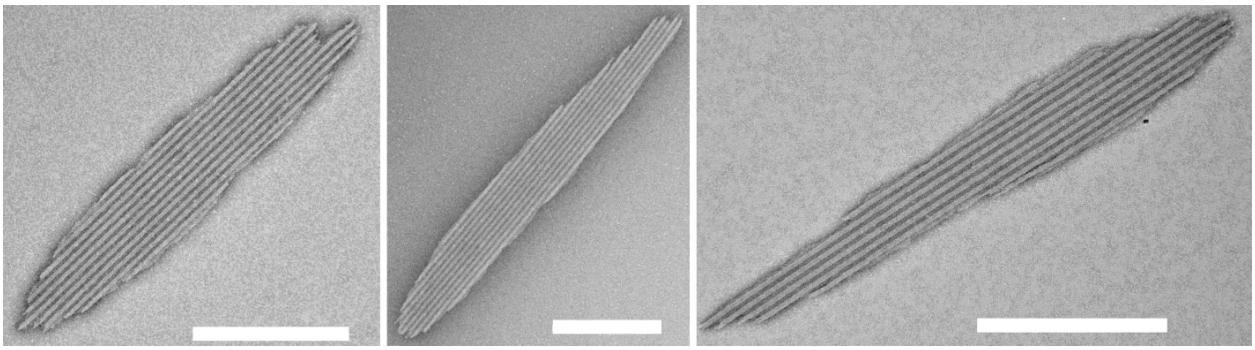

Figure S3. **More TEM images of typical DNA brick crystals with 25.3-nm trench periodicity along x direction**. The scale bars are 500 nm.

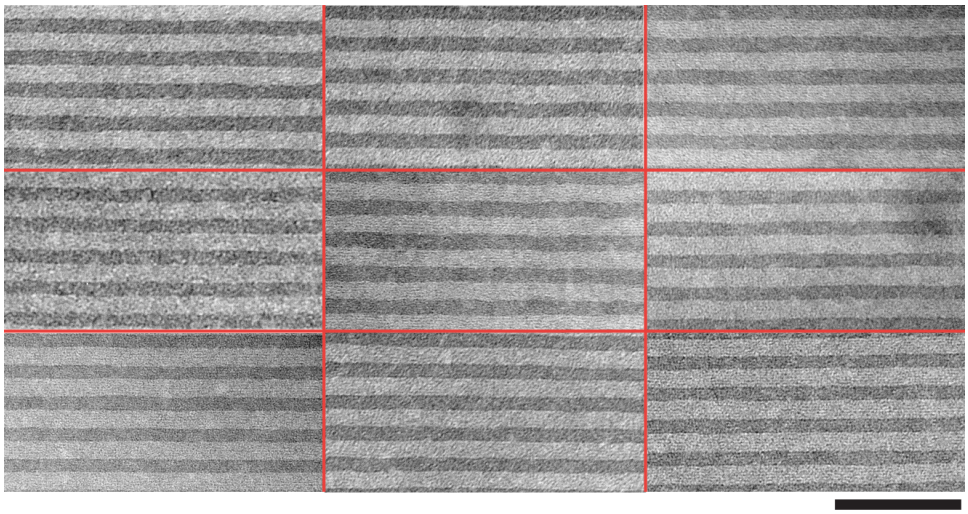

Figure S4. **Zoomed-in TEM images for 9 randomly selected DNA brick crystals with 25.3-nm trench periodicity along x direction**. The scale bar is 100 nm.

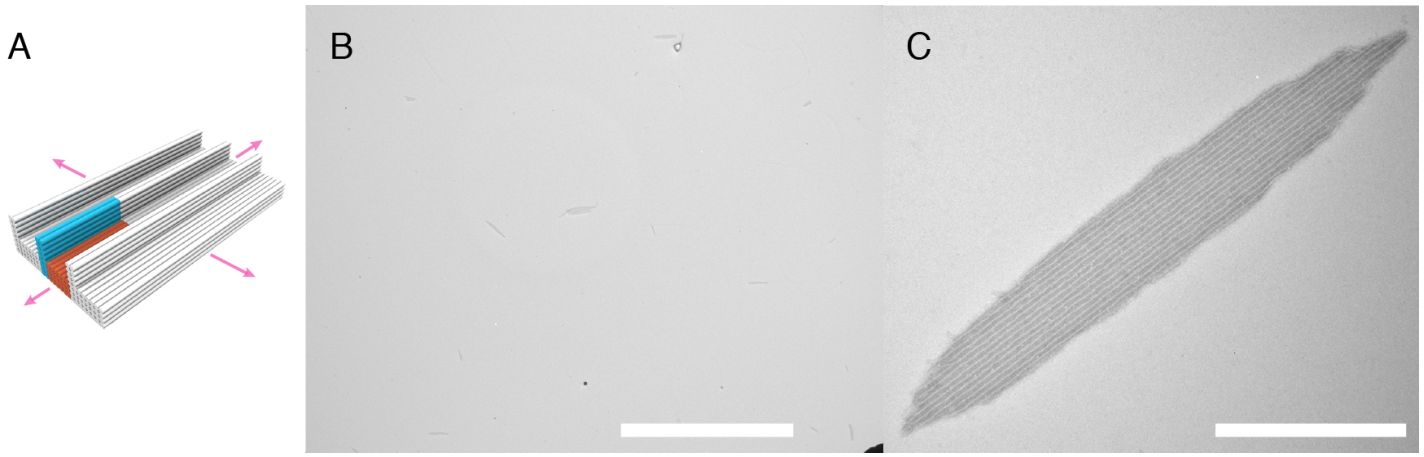

Figure S5. **Design (A), zoomed-out (B), and zoomed-in (C) TEM images of the DNA brick crystal with 16.8-nm trench periodicity along x direction**. Feature-repeating unit of the designed crystal is denoted using colored bundles. Pink arrows in A represent the growth directions of the crystal template. DNA brick crystals are diluted 500 folds prior to imaging. The scale bar in B is 10 μm. The scale bar in C is 500 nm.

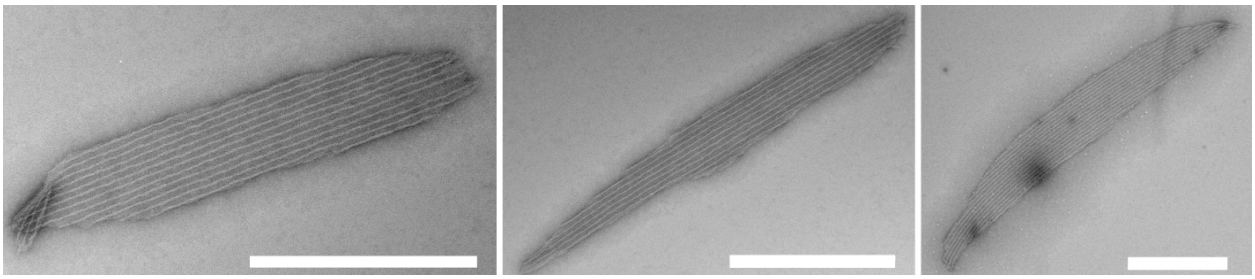

Figure S6. **More TEM images of typical DNA brick crystals with 16.8-nm trench periodicity along x direction**. The scale bars are 500 nm.

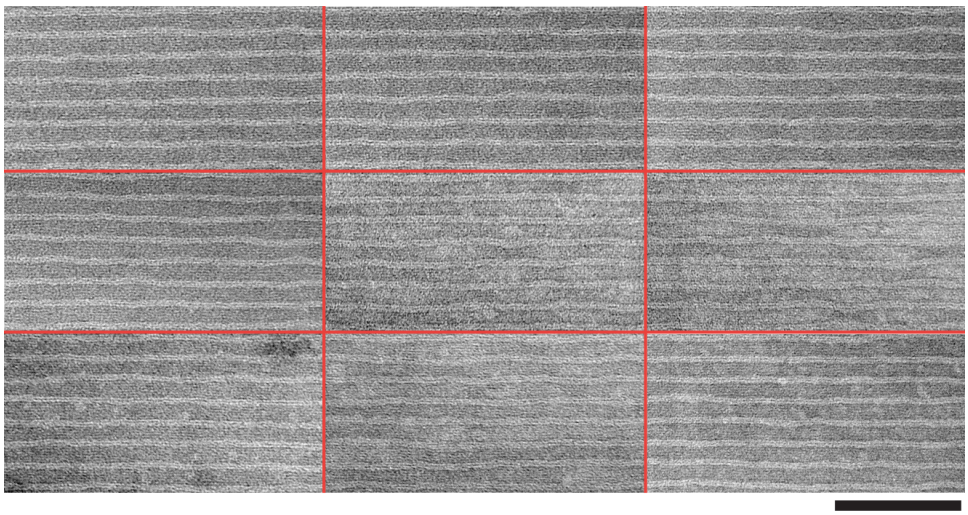

Figure S7. **Zoomed-in TEM images for 9 randomly selected DNA brick crystals with 16.8-nm trench periodicity along x direction**. The scale bar is 100 nm.

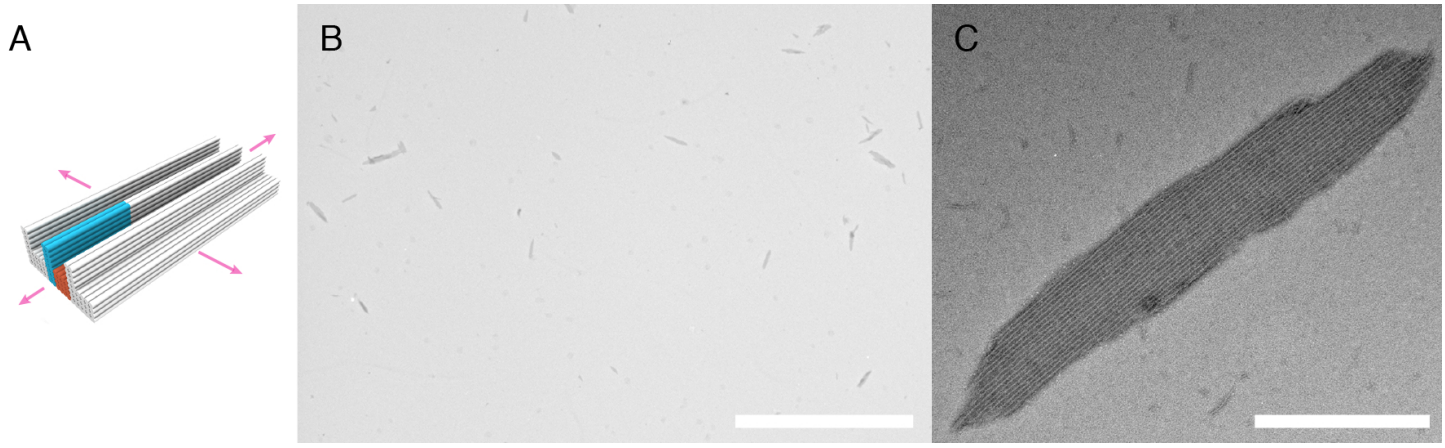

Figure S8. **Design (A), zoomed-out (B), and zoomed-in (C) TEM images of the DNA brick crystal with 12.7-nm trench periodicity along x direction**. Feature-repeating unit of the designed crystal is denoted using colored bundles. Pink arrows in A represent the growth directions of the crystal template. DNA brick crystals are diluted 500 folds prior to imaging. The scale bar in B is 10 μm. The scale bar in C is 500 nm.

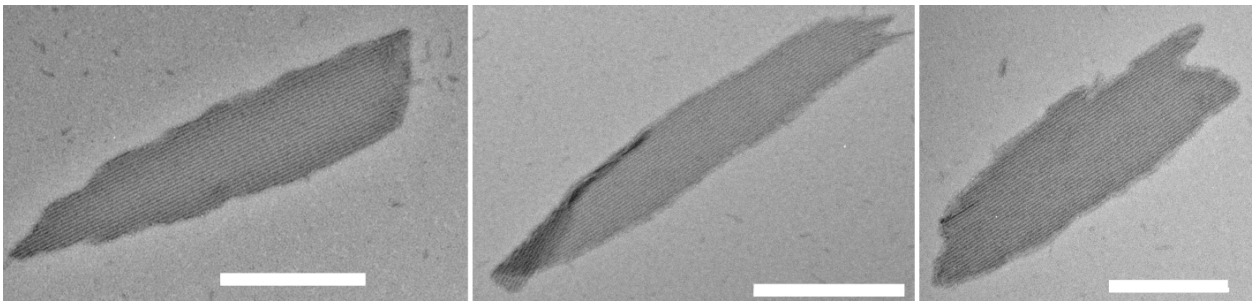

Figure S9. **More TEM images of typical DNA brick crystals with 12.7-nm trench periodicity along x direction**. The scale bars are 500 nm.

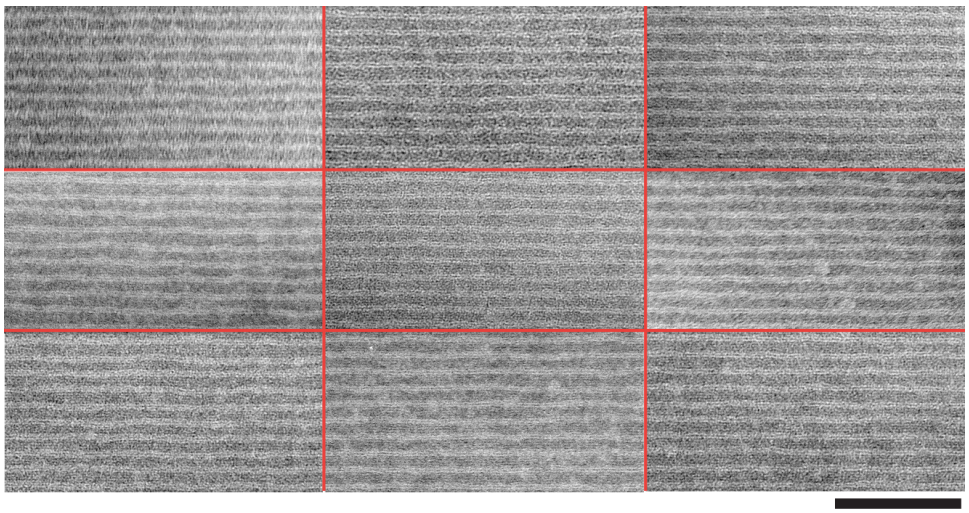

Figure S10. **Zoomed-in TEM images for 9 randomly selected DNA brick crystals with 12.7-nm trench periodicity along x direction**. The scale bar is 100 nm.

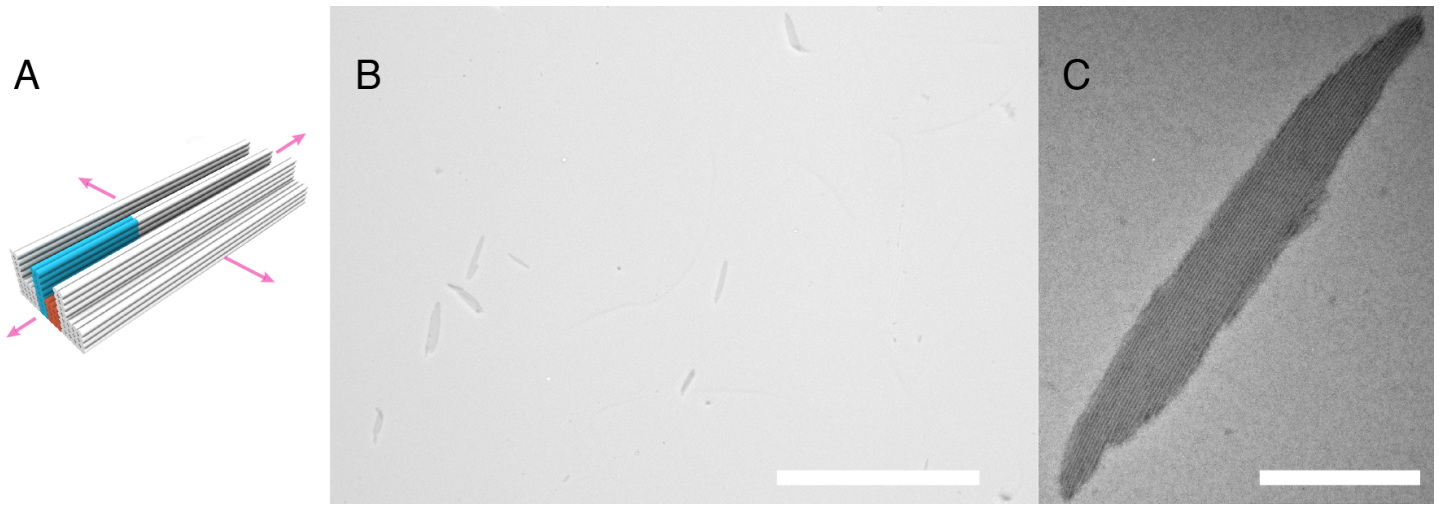

Figure S11. **Design (A), zoomed-out (B), and zoomed-in (C) TEM images of the DNA brick crystal with 10.6-nm trench periodicity along x direction**. Feature-repeating unit of the designed crystal is denoted using colored bundles. Pink arrows in A represent the growth directions of the crystal template. DNA brick crystals are diluted 500 folds prior to imaging. The scale bar in B is 10 μm. The scale bar in C is 500 nm.

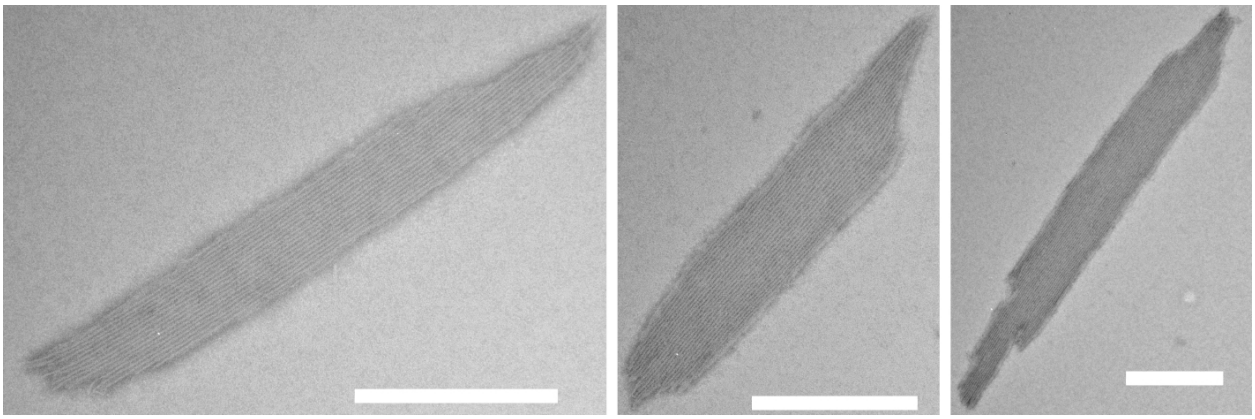

Figure S12. **More TEM images of typical DNA brick crystals with 10.6-nm trench periodicity along x direction**. The scale bars are 500 nm.

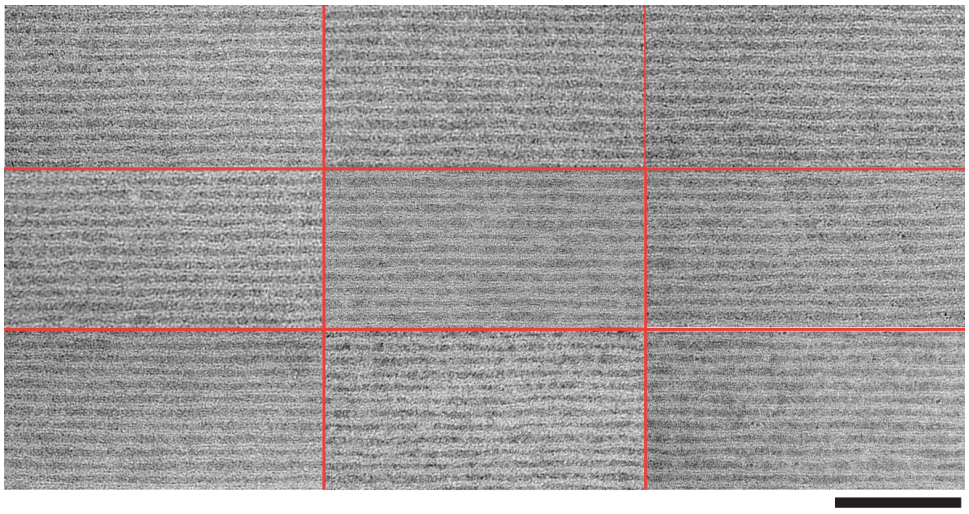

Figure S13. **Zoomed-in TEM images for 9 randomly selected DNA brick crystals with 10.6-nm trench periodicity along x direction**. The scale bar is 100 nm.

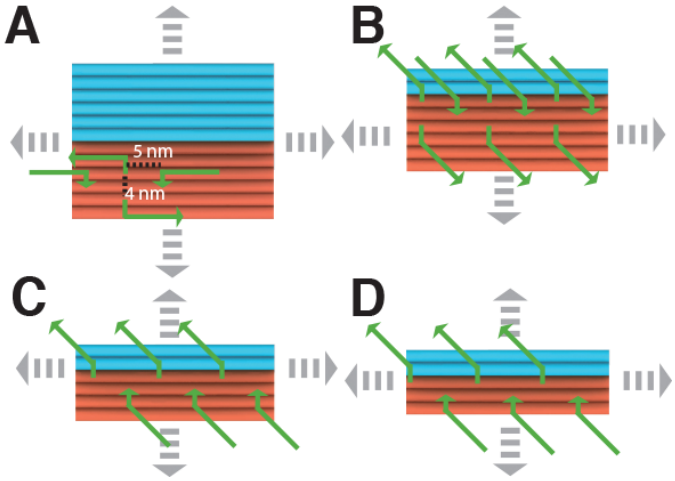

Figure S14. **Designs of DNA handles on DNA brick crystals**. The blue and orange colored bundles represent a feature-repeating unit of designed DNA brick crystals with 25.3-nm (A), 16.8-nm (B), 12.7-nm (C), and 10.6-nm (D) trench periodicity along x direction. Specifically, the blue bundles are the sidewalls of DNA nanotrench; and the orange bundles are the bottom layer of DNA nanotrench. Green arrows denote the DNA handles. The gray arrows represent the growth directions of the crystal template. The white numbers indicate the spacing between DNA handles in A.

S4 Design and characterization of CNT arrays assembled on DNA brick crystal templates

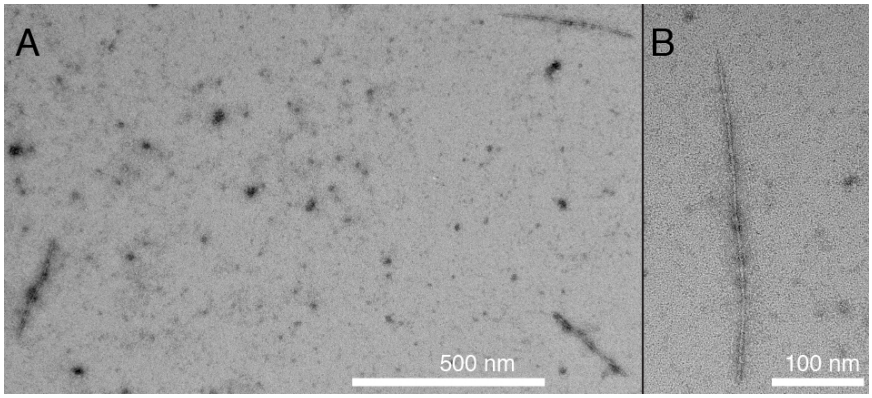

Figure S15. **Zoomed-out (A) and zoomed-in (B) TEM images of the DNA-wrapped CNTs**. The scale bar in A is 500 nm. The scale bar in B is 100 nm.

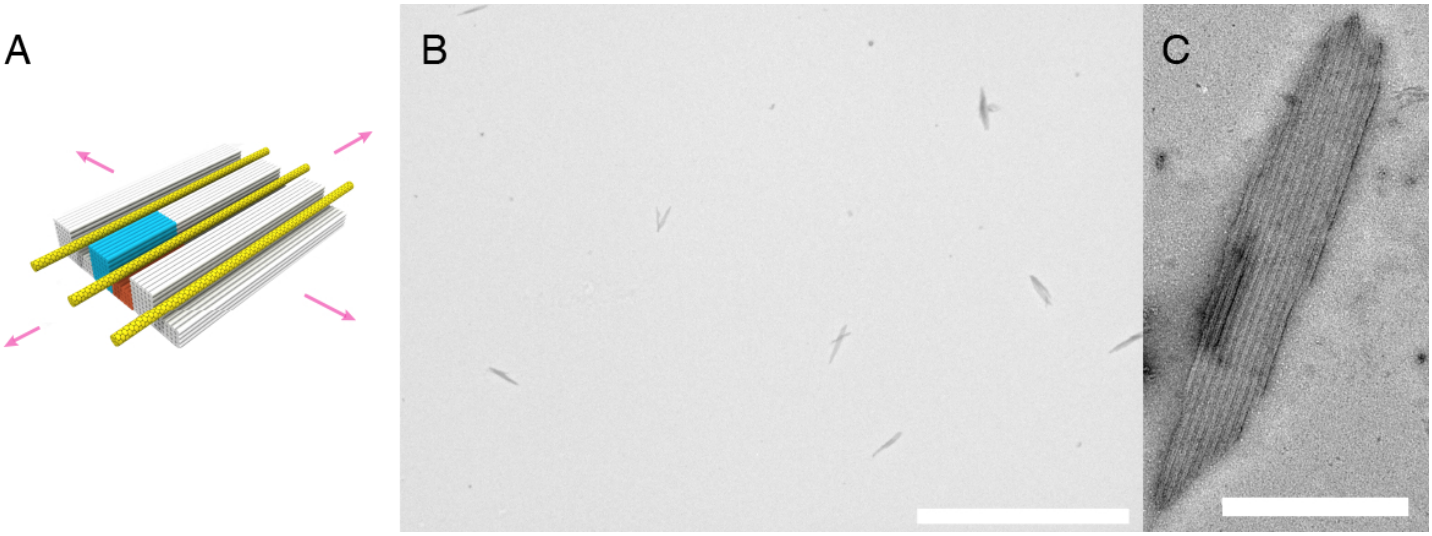

Figure S16. **Design (A), zoomed-out (B) and zoomed-in (C) TEM images of the CNT arrays assembled on DNA brick crystal with 24.1-nm trench periodicity along x direction**. Feature-repeating unit of the designed brick crystal template is denoted using colored bundles (blue and orange). Yellow rods denote the CNTs. Pink arrows in A represent the growth directions of the crystal template. CNT-decorated DNA brick crystals are diluted 6 folds prior to imaging. The scale bar in B is 10 μm. The scale bar in C is 500 nm.

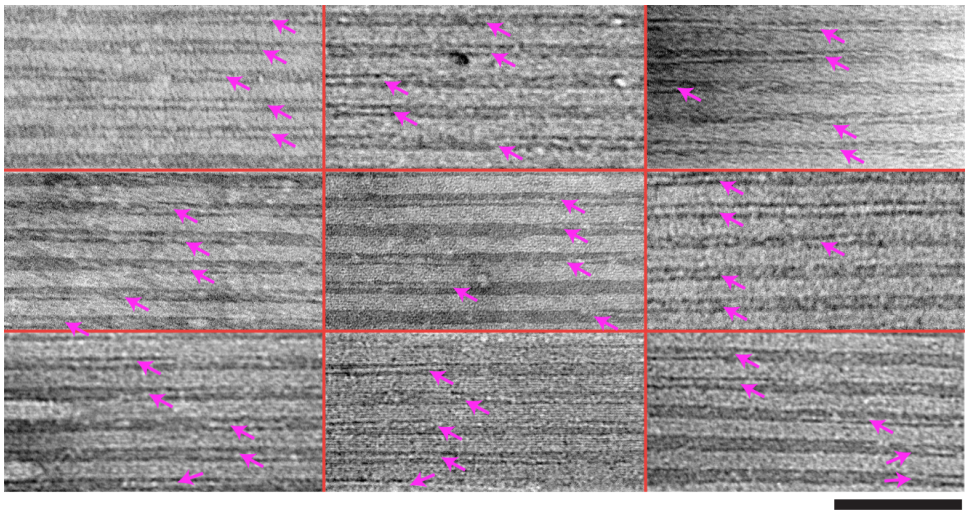

Figure S17. **Zoomed-in TEM images for 9 randomly selected CNT arrays assembled on DNA brick crystals with 24.1-nm trench periodicity along x direction**. Pink arrows indicate the CNTs within the DNA nanotrenches. The scale bar is 100 nm.

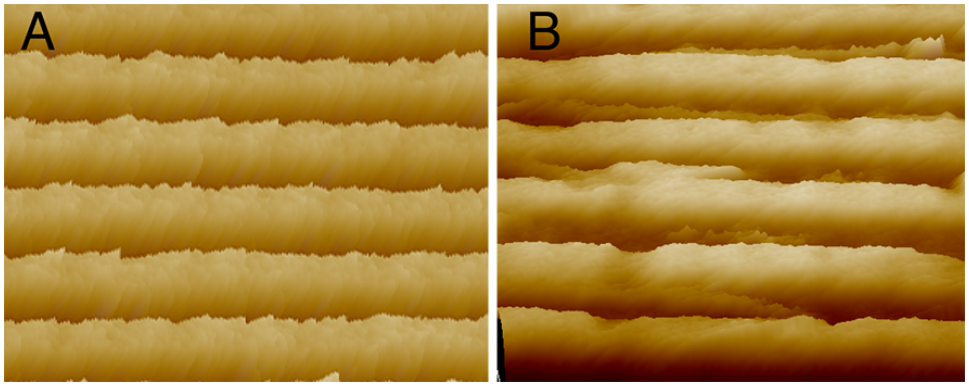

Figure S18. **Tilted AFM images for DNA brick crystals before (A) and after (B) CNT assembly.**

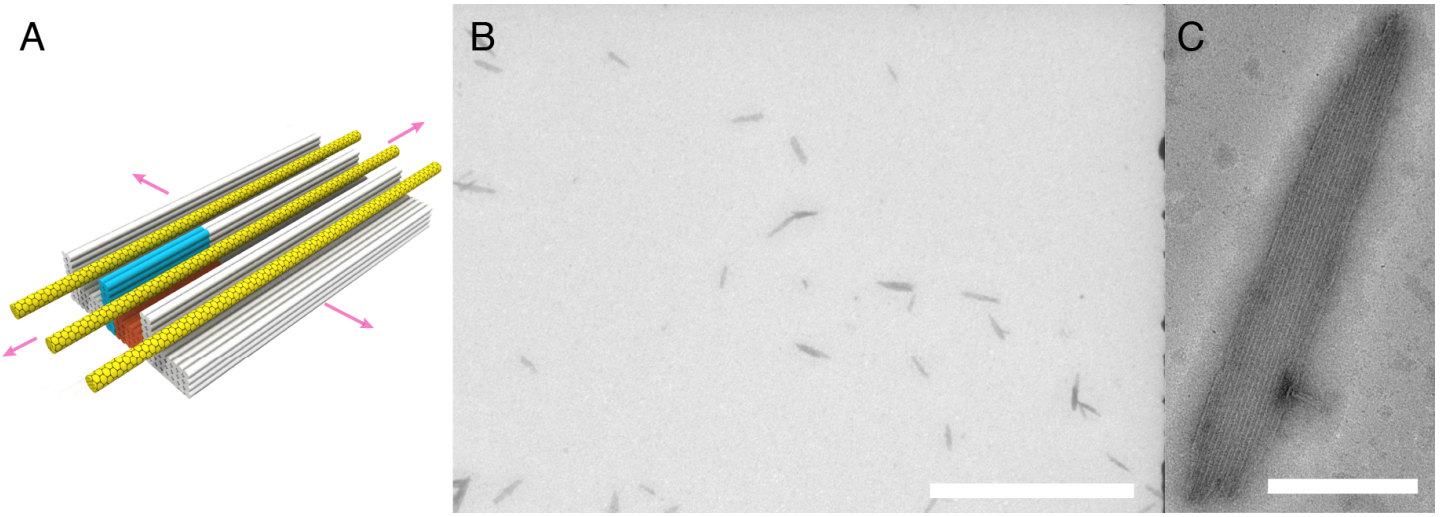

Figure S19. **Design (A), zoomed-out (B) and zoomed-in (C) TEM images of the CNT arrays assembled on DNA brick crystal with 16.8-nm trench periodicity along x direction**. Feature-repeating unit of the designed brick crystal template is denoted using colored bundles (blue and orange). Yellow rods denote the CNTs. Pink arrows in A represent the growth directions of the crystal template. CNT-decorated DNA brick crystals are diluted 6 folds prior to imaging. The scale bar in B is 10 μm. The scale bar in C is 500 nm.

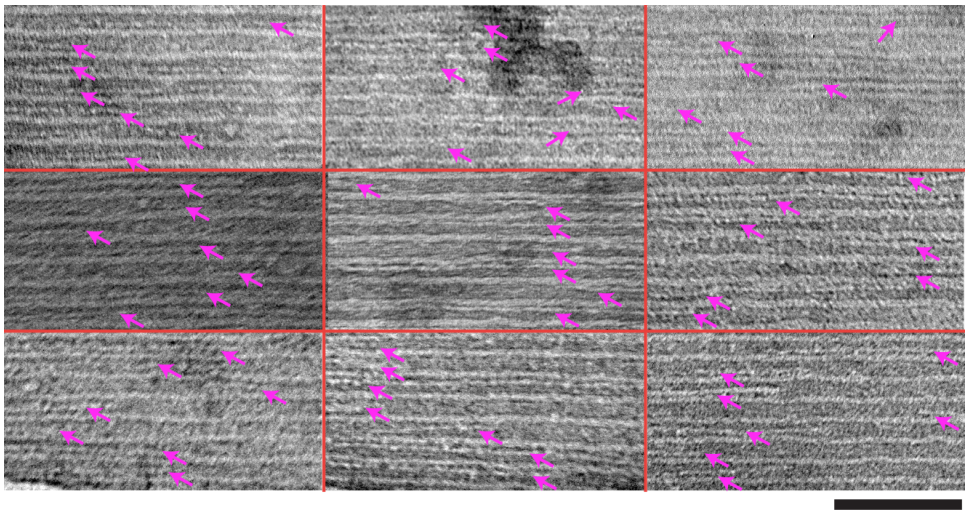

Figure S20. **Zoomed-in TEM images for 9 randomly selected CNT arrays assembled on DNA brick crystals with 16.8-nm trench periodicity along x direction**. Pink arrows indicate the CNTs within the DNA nanotrenches. The scale bar is 100 nm.

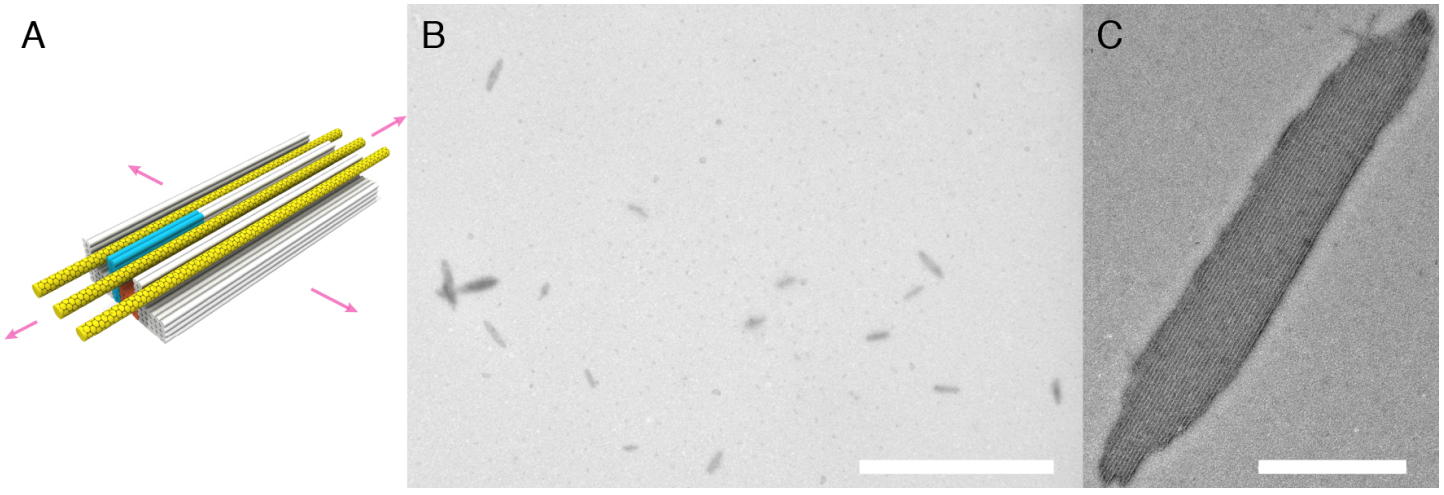

Figure S21. **Design (A), zoomed-out (B) and zoomed-in (C) TEM images of the CNT arrays assembled on DNA brick crystal with 12.6-nm trench periodicity along x direction**. Feature-repeating unit of the designed crystal is denoted using colored bundles (blue and orange). Yellow rods denote the CNTs. Pink arrows in A represent the growth directions of the crystal template. CNT-decorated DNA brick crystals are diluted 6 folds prior to imaging. The scale bar in B is 10 μm. The scale bar in C is 500 nm.

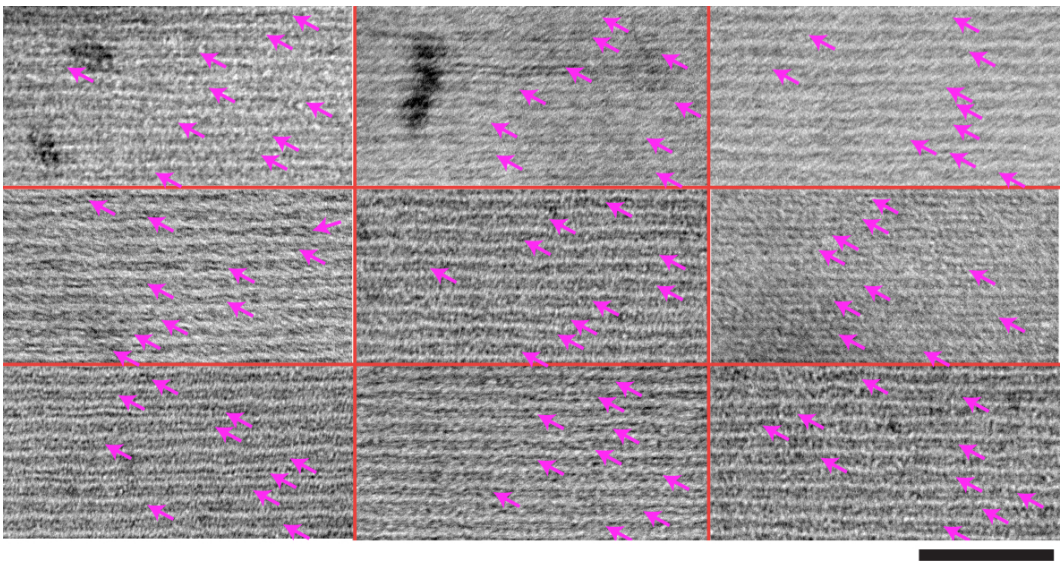

Figure S22. **Zoomed-in TEM images for 9 randomly selected CNT arrays assembled on DNA brick crystals with 12.6-nm trench periodicity along x direction**. Pink arrows indicate the CNTs within the DNA nanotrenches. The scale bar is 100 nm.

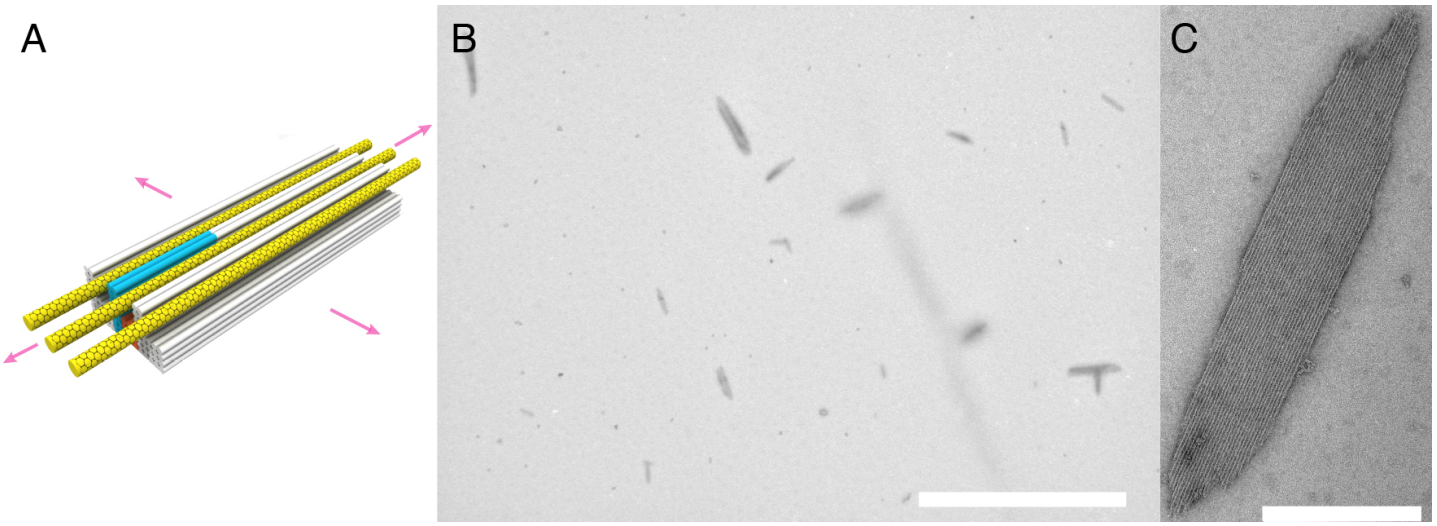

Figure S23. **Design (A), zoomed-out (B) and zoomed-in (C) TEM images of the CNT arrays assembled on DNA brick crystal with 10.4-nm trench periodicity along x direction**. Feature-repeating unit of the designed crystal is denoted using colored bundles (blue and orange). Yellow rods denote the CNTs. Pink arrows in A represent the growth directions of the crystal template. CNT-decorated DNA brick crystals are diluted 6 folds prior to imaging. The scale bar in B is 10 μm. The scale bar in C is 500 nm.

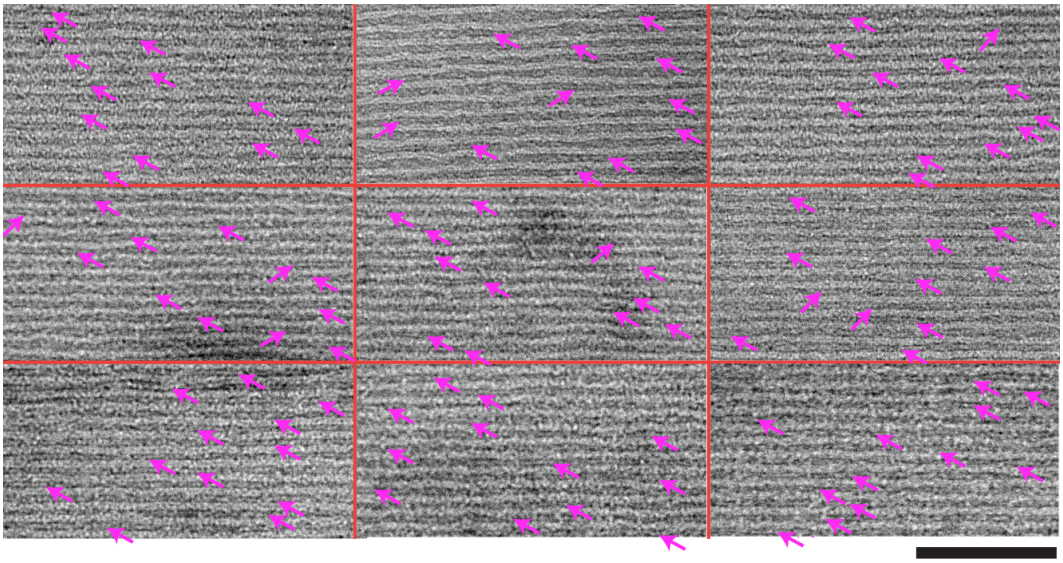

Figure S24. **Zoomed-in TEM images for 9 randomly selected CNT arrays assembled on DNA brick crystals with 10.4-nm trench periodicity along x direction**. Pink arrows indicate the CNTs within the DNA nanotrenches. The scale bar is 100 nm.

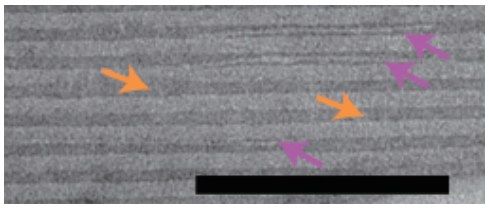

Figure S25. **TEM image for the assembly defect**. Pink arrows indicate the CNTs within the DNA nanotrenches. Orange arrows indicate the empty DNA nanotrenches, which are counted as the assembly defects. The stoichiometry between CNTs and the DNA brick crystals is one third of the optimal value (that is, off-stoichiometry product). The scale bar is 200 nm.

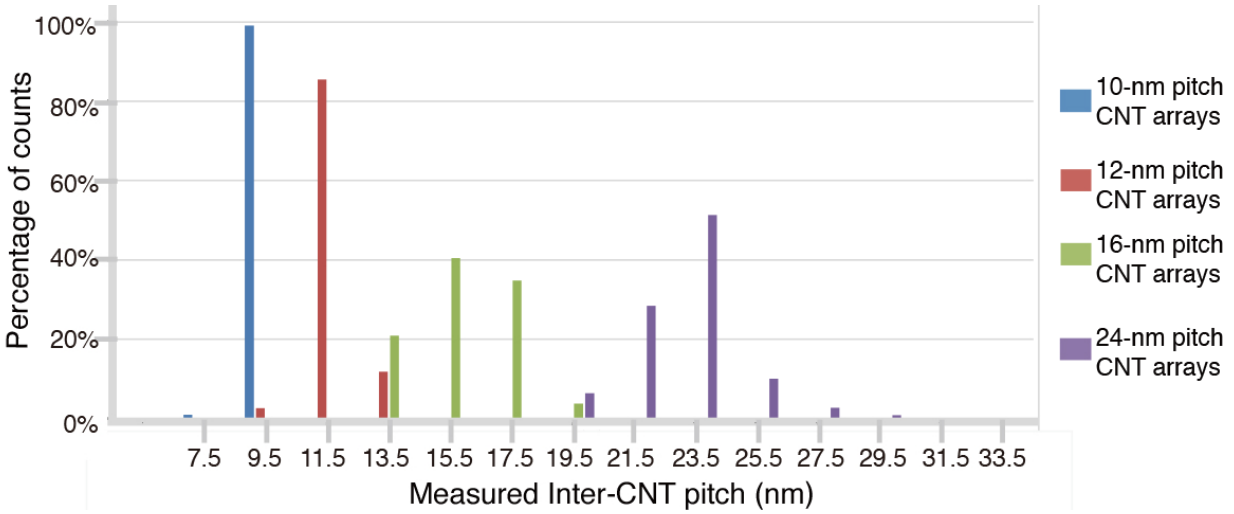

Figure S26. **Distribution of inter-CNT pitches**. At each prescribed inter-CNT pitch (denoted as blue, red, green or purple color), the percentage of counts indicated the distribution of experimentally observed pitch values along x direction. The inter-CNT pitch was measured from the TEM images of 10 randomly selected DNA brick crystals. For each prescribed inter-CNT pitch, the numbers of total counted CNTs were around 50—300. Because the DNA brick crystals exhibited uneven width, the CNT counts varied from template to template. And at similar crystal width, DNA brick crystals with smaller pitch (i.e. 10.4 nm) had more CNT counts than that at larger pitch (i.e. 25.2 nm). For every two neighboring CNTs, we measured three different positions along the longitudinal axis of CNTs. The distribution of inter-CNT pitches revealed the assembly precision of CNTs within DNA nanotrenches. When the trench width was 6 nm, we noticed that the majority (>95%) of CNTs exhibited pitch variation less than 1 nm, indicative of sub-2 nm positioning precision within the narrow DNA nanotrenches.

S4.1 Extended technical description on different approaches for making high-density CNT arrays

Mathematically, CNT arrays with 10-nm inter-CNT pitch exhibit local density of 100 CNTs/μm. However, CNT density does not reflect the array uniformity. Different from the uniform inter-CNT pitch demonstrated in the manuscript, other approaches for preparing CNT arrays with 100 CNTs/μm or higher density, including the repeated transfers (*11*), directional growth (*35*), and Langmuir-Schaefer approach (*3, 36*), exhibit irregular array morphologies. Uneven inter-CNT pitch (ranging from 2 nm to a few micrometers in the same array) or random CNT orientation and the resulted crossing CNTs are often observed in these thin-film approaches.

It has been reported that IDC value (representative of CNT disorder) impacts the gate delay and the energy increase per cycle at 16 nm node (*37*). Their simulations indicate that, simply by reducing the IDC value from 0.5 to 0.1, both the gate delay and the energy increase per cycle improve by more than 50%. So smaller IDC values (higher array uniformity) lead to better device performance. However, many previous reports on the high-density CNT arrays exhibit IDC values higher than 0.5 (*11*).

At ultra-scaled technology nodes, semiconductor industry typically has a high standard on the uniformity of the semiconductor channels. In Si CMOS at 14 nm technology node, the fin pitch variation is typically less than 3 nm, leading to an IDC value smaller than 0.01. This value is comparable to our demonstration for CNT channels.

Based on the discussions above, when using the parallel CNT arrays in the ultra-scaled technology nodes, the maximum allowed pitch variation and the IDC value should be similar to our demonstration.

S5 DNA removal and FET construction

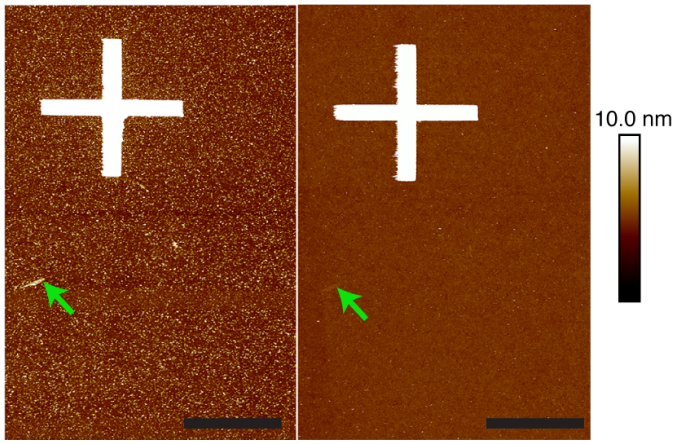

Figure S27. **Zoomed-out AFM images for the deposited substrate before (left) and after (right) the liftoff process to remove salt residues and surface DNAs**. Both images are scanned at the identical regions on the substrate. The bright cross shapes on both images are the fine alignment fiducial markers written with e-beam lithography. The scale bars are 3 μm. The bright spots in the left AFM image are salt residues. The green arrows indicate the CNT-decorated DNA brick crystal before (left) and after (right) the liftoff process. After the liftoff process, most of salt residues (bright spots in the left) and surface DNAs (green arrow in the left) with height higher than 8 nm were removed (evidenced by the absence of bright spots and lowered heights of DNA area in the right image). The residual height was around 1 nm, as indicated by the height change in AFM.

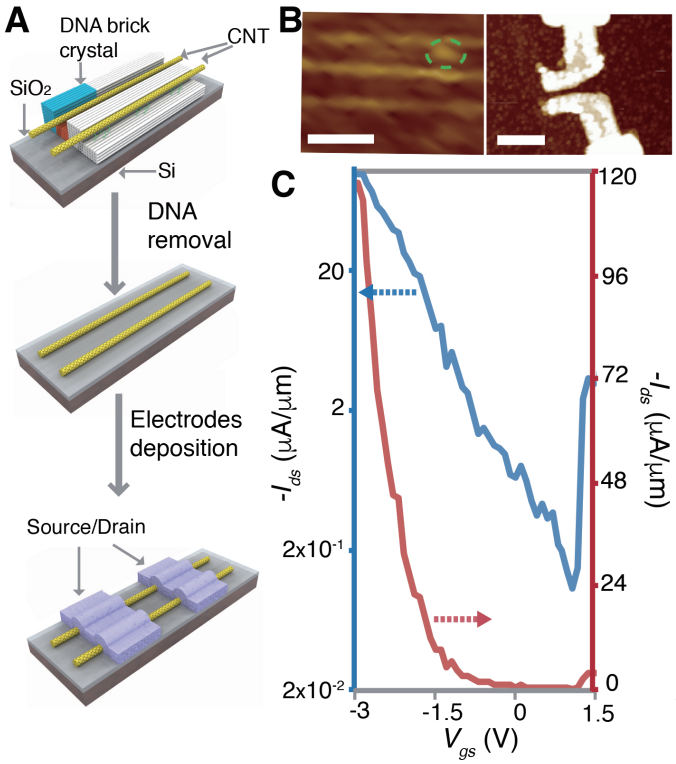

Figure S28. **Constructing bottom-gated CNT FETs at 24-nm inter-CNT pitch**. (**A**) Design schematic for DNA removal and depositing the source/drain electrodes. The blue and orange colored bundles together represent a structural repeating unit of DNA brick crystals with 24 nm periodicity along the x direction. The yellow rods represent CNTs. The purple objects represent the deposited electrodes. (**B**) Left, AFM image of the assembled CNT arrays after DNA removal. The scale bar is 50 nm. The green circle indicates one residue after DNA removal. Right, AFM image of the fabricated FET. The scale bar is 300 nm. CNTs are not visible in the AFM image due to the their small diameter compared to the electrode thickness. (**C**)The $I_{ds}-V_{gs}$ curve plotted in both logarithmic (left axis, blue) and linear (right axis, red) scales at V_{ds} of -0.5 V for a dual-channel CNT FET. I_{ds} is normalized to the inter-CNT pitch.

References and Notes

1. G. S. Tulevski, A. D. Franklin, D. Frank, J. M. Lobez, Q. Cao, H. Park, A. Afzali, S.-J. Han, J. B. Hannon, W. Haensch, Toward high-performance digital logic technology with carbon nanotubes. *ACS Nano* **8**, 8730–8745 (2014). doi:10.1021/nn503627h Medline

2. Z. Hu, J. M. M. L. Comeras, H. Park, J. Tang, A. Afzali, G. S. Tulevski, J. B. Hannon, M. Liehr, S.-J. Han, Physically unclonable cryptographic primitives using self-assembled carbon nanotubes. *Nat. Nanotechnol.* **11**, 559–565 (2016). doi:10.1038/nnano.2016.1 Medline

3. Q. Cao, S. J. Han, G. S. Tulevski, Y. Zhu, D. D. Lu, W. Haensch, Arrays of single-walled carbon nanotubes with full surface coverage for high-performance electronics. *Nat. Nanotechnol.* **8**, 180–186 (2013). doi:10.1038/nnano.2012.257 Medline

4. Q. Cao, S.-J. Han, G. S. Tulevski, Fringing-field dielectrophoretic assembly of ultrahigh-density semiconducting nanotube arrays with a self-limited pitch. *Nat. Commun.* **5**, 5071 (2014). doi:10.1038/ncomms6071 Medline

5. G. J. Brady, A. J. Way, N. S. Safron, H. T. Evensen, P. Gopalan, M. S. Arnold, Quasi-ballistic carbon nanotube array transistors with current density exceeding Si and GaAs. *Sci. Adv.* **2**, e1601240 (2016). doi:10.1126/sciadv.1601240 Medline

6. X. He, W. Gao, L. Xie, B. Li, Q. Zhang, S. Lei, J. M. Robinson, E. H. Hároz, S. K. Doorn, W. Wang, R. Vajtai, P. M. Ajayan, W. W. Adams, R. H. Hauge, J. Kono, Wafer-scale monodomain films of spontaneously aligned single-walled carbon nanotubes. *Nat. Nanotechnol.* **11**, 633–638 (2016). doi:10.1038/nnano.2016.44 Medline

7. J. Wu, L. Jiao, A. Antaris, C. L. Choi, L. Xie, Y. Wu, S. Diao, C. Chen, Y. Chen, H. Dai, Self-assembly of semiconducting single-walled carbon nanotubes into dense, aligned rafts. *Small* **9**, 4142–4148 (2013). doi:10.1002/smll.201301547 Medline

8. S.-P. Han, H. T. Maune, R. D. Barish, M. Bockrath, W. A. Goddard 3rd, DNA-linker-induced surface assembly of ultra dense parallel single walled carbon nanotube arrays. *Nano Lett.* **12**, 1129–1135 (2012). doi:10.1021/nl201818u Medline

9. A. Mangalum, M. Rahman, M. L. Norton, Site-specific immobilization of single-walled carbon nanotubes onto single and one-dimensional DNA origami. *J. Am. Chem. Soc.* **135**, 2451–2454 (2013). doi:10.1021/ja312191a Medline

10. G. J. Brady, K. R. Jinkins, M. S. Arnold, Channel length scaling behavior in transistors based on individual versus dense arrays of carbon nanotubes. *J. Appl. Phys.* **122**, 124506 (2017). doi:10.1063/1.4996586

11. M. M. Shulaker *et al*., High-performance carbon nanotube field-effect transistors, in *2014 IEEE International Electron Devices Meeting* (IEEE, 2014), pp. 33.6.1–33.6.4.

12. N. C. Seeman, Nucleic acid junctions and lattices. *J. Theor. Biol.* **99**, 237–247 (1982). doi:10.1016/0022-5193(82)90002-9 Medline

13. N. C. Seeman, DNA in a material world. *Nature* **421**, 427–431 (2003). doi:10.1038/nature01406 Medline

14. P. W. K. Rothemund, Folding DNA to create nanoscale shapes and patterns. *Nature* **440**, 297–302 (2006). doi:10.1038/nature04586 Medline

15. S. M. Douglas, H. Dietz, T. Liedl, B. Högberg, F. Graf, W. M. Shih, Self-assembly of DNA into nanoscale three-dimensional shapes. *Nature* **459**, 414–418 (2009). doi:10.1038/nature08016 Medline

16. Y. Ke, L. L. Ong, W. M. Shih, P. Yin, Three-dimensional structures self-assembled from DNA bricks. *Science* **338**, 1177–1183 (2012). doi:10.1126/science.1227268 Medline

17. Y. Ke, L. L. Ong, W. Sun, J. Song, M. Dong, W. M. Shih, P. Yin, DNA brick crystals with prescribed depths. *Nat. Chem.* **6**, 994–1002 (2014). doi:10.1038/nchem.2083 Medline

18. S. P. Surwade, F. Zhou, B. Wei, W. Sun, A. Powell, C. O'Donnell, P. Yin, H. Liu, Nanoscale growth and patterning of inorganic oxides using DNA nanostructure templates. *J. Am. Chem. Soc.* **135**, 6778–6781 (2013). doi:10.1021/ja401785h Medline

19. X. Liu, F. Zhang, X. Jing, M. Pan, P. Liu, W. Li, B. Zhu, J. Li, H. Chen, L. Wang, J. Lin, Y. Liu, D. Zhao, H. Yan, C. Fan, Complex silica composite nanomaterials templated with DNA origami. *Nature* **559**, 593–598 (2018). doi:10.1038/s41586-018-0332-7 Medline

20. Z. Jin, W. Sun, Y. Ke, C.-J. Shih, G. L. C. Paulus, Q. Hua Wang, B. Mu, P. Yin, M. S. Strano, Metallized DNA nanolithography for encoding and transferring spatial information for graphene patterning. *Nat. Commun.* **4**, 1663 (2013). doi:10.1038/ncomms2690 Medline

21. A. Kuzyk, R. Schreiber, Z. Fan, G. Pardatscher, E.-M. Roller, A. Högele, F. C. Simmel, A. O. Govorov, T. Liedl, DNA-based self-assembly of chiral plasmonic nanostructures with tailored optical response. *Nature* **483**, 311–314 (2012). doi:10.1038/nature10889 Medline

22. P. Zhan, T. Wen, Z. G. Wang, Y. He, J. Shi, T. Wang, X. Liu, G. Lu, B. Ding, DNA origami directed assembly of gold bowtie nanoantennas for single-molecule surface-enhanced Raman scattering. *Angew. Chem. Int. Ed.* **57**, 2846–2850 (2018). doi:10.1002/anie.201712749 Medline

23. J. B. Knudsen, L. Liu, A. L. Bank Kodal, M. Madsen, Q. Li, J. Song, J. B. Woehrstein, S. F. J. Wickham, M. T. Strauss, F. Schueder, J. Vinther, A. Krissanaprasit, D. Gudnason, A. A. A. Smith, R. Ogaki, A. N. Zelikin, F. Besenbacher, V. Birkedal, P. Yin, W. M. Shih, R. Jungmann, M. Dong, K. V. Gothelf, Routing of individual polymers in designed patterns. *Nat. Nanotechnol.* **10**, 892–898 (2015). doi:10.1038/nnano.2015.190 Medline

24. H. T. Maune, S. P. Han, R. D. Barish, M. Bockrath, W. A. Goddard III, P. W. K. Rothemund, E. Winfree, Self-assembly of carbon nanotubes into two-dimensional geometries using DNA origami templates. *Nat. Nanotechnol.* **5**, 61–66 (2010). doi:10.1038/nnano.2009.311 Medline

25. H. Pei, R. Sha, X. Wang, M. Zheng, C. Fan, J. W. Canary, N. C. Seeman, Organizing end-site-specific SWCNTs in specific loci using DNA. *J. Am. Chem. Soc.* **141**, 11923–11928 (2019). doi:10.1021/jacs.9b03432 Medline

26. See supplementary materials.

27. M. Zheng, A. Jagota, E. D. Semke, B. A. Diner, R. S. McLean, S. R. Lustig, R. E. Richardson, N. G. Tassi, DNA-assisted dispersion and separation of carbon nanotubes. *Nat. Mater.* **2**, 338–342 (2003). doi:10.1038/nmat877 Medline

28. Z. Zhao, Y. Liu, H. Yan, DNA origami templated self-assembly of discrete length single wall carbon nanotubes. *Org. Biomol. Chem.* **11**, 596–598 (2013). doi:10.1039/C2OB26942B Medline

29. W. Sun, E. Boulais, Y. Hakobyan, W. L. Wang, A. Guan, M. Bathe, P. Yin, Casting inorganic structures with DNA molds. *Science* **346**, 1258361 (2014). doi:10.1126/science.1258361 Medline

30. *The International Technology Roadmap for Semiconductors: 2013*; www.semiconductors.org/resources/2013-international-technology-roadmap-for-semiconductors-itrs/.

31. G. Hills, M. G. Bardon, G. Doornbos, D. Yakimets, P. Schuddinck, R. Baert, D. Jang, L. Mattii, S. M. Y. Sherazi, D. Rodopoulos, R. Ritzenthaler, C.-S. Lee, A. V.-Y. Thean, I. Radu, A. Spessot, P. Debacker, F. Catthoor, P. Raghavan, M. M. Shulaker, H.-S. P. Wong, S. Mitra, Understanding energy efficiency benefits of carbon nanotube field-effect transistors for digital VLSI. *IEEE Trans. NanoTechnol.* **17**, 1259–1269 (2018). doi:10.1109/TNANO.2018.2871841

32. M. Zhao, Y. Chen, K. Wang, Z. Zhang, J. K. Streit, J. A. Fagan, J. Tang, M. Zheng, C. Yang, Z. Zhu, W. Sun, DNA-directed nanofabrication of high-performance carbon nanotube field-effect transistors. *Science* **368**, 878–881 (2020).

33. H. Gui, J. K. Streit, J. A. Fagan, A. R. Hight Walker, C. Zhou, M. Zheng, Redox sorting of carbon nanotubes. *Nano Lett.* **15**, 1642–1646 (2015). doi:10.1021/nl504189p Medline

34. J. K. Streit, J. A. Fagan, M. Zheng, A Low Energy Route to DNA-Wrapped Carbon Nanotubes via Replacement of Bile Salt Surfactants. *Anal. Chem.* **89**, 10496–10503 (2017). doi:10.1021/acs.analchem.7b02637 Medline

35. Y. Hu, L. Kang, Q. Zhao, H. Zhong, S. Zhang, L. Yang, Z. Wang, J. Lin, Q. Li, Z. Zhang, L. Peng, Z. Liu, J. Zhang, Growth of high-density horizontally aligned SWNT arrays using Trojan catalysts. *Nat. Commun.* **6**, 6099 (2015). doi:10.1038/ncomms7099 Medline

36. Q. Cao, J. Tersoff, D. B. Farmer, Y. Zhu, S.-J. Han, Carbon nanotube transistors scaled to a 40-nanometer footprint. *Science* **356**, 1369–1372 (2017). doi:10.1126/science.aan2476 Medline

37. J. Zhang, N. Patil, H.-S. P. Wong, S. Mitra, Overcoming carbon nanotube variations through co-optimized technology and circuit design, *IEEE Int. Electron Devices Meeting in San Francisco CA* 4.6.1-4.6.4 (2011).